A Weak Donor–Strong Acceptor Strategy to Design Ideal Polymers for Organic Solar Cells

Huaxing Zhou,[†] Liqiang Yang,[‡] Sarah Stoneking,[†] and Wei You*[,†,‡]

Department of Chemistry, University of North Carolina at Chapel Hill, Chapel Hill, North Carolina 27599-3290, and Curriculum in Applied Sciences and Engineering, University of North Carolina at Chapel Hill, Chapel Hill, North Carolina 27599-3287

ABSTRACT Polymers to be used in bulk heterojunction (BHJ) solar cells should maintain a low highest occupied molecular orbital (HOMO) energy level as well as a narrow band gap in order to maximize the open circuit voltage (V_{oc}) and the short circuit current (J_{sc}). To concurrently lower the HOMO energy level and the band gap, we propose to modify the donor–acceptor low band gap polymer strategy by constructing alternating copolymers incorporating a "weak donor" and a "strong acceptor". As a result, the "weak donor" should help maintain a low HOMO energy level while the "strong acceptor" should reduce the band gap via internal charge transfer (ICT). This concept was examined by constructing a library of polymers employing the naphtho[2,1-*b*:3,4-*b*']dithiophene (**NDT**) unit as the weak donor, and benzothiadiazole (**BT**) as the strong acceptor. **PNDT-BT**, designed under the "weak donor–strong acceptor" strategy, demonstrated both a low HOMO energy level of −5.35 eV and a narrow band gap of 1.59 eV. As expected, a noticeably high V_{oc} of 0.83 V was obtained from the BHJ device of **PNDT-BT** blended with PCBM. However, the J_{sc} (~3 mA/cm^2) was significantly lower than the maximum expected current from such a low band gap material, which limited the observed efficiency to 1.27% (with a 70 nm thin film). Further improvements in the efficiency are expected from these materials if new strategies can be identified to (a) increase the molecular weight and (b) improve the hole mobility while still maintaining a low HOMO energy level and a narrow band gap.

KEYWORDS: conjugated polymers • solar cell • fullerene • bulk heterojunction • thin film devices • solution processing

INTRODUCTION

To date, the most successful method to construct the active layer of a polymer solar cell is to blend a photoactive polymer and an electron acceptor in a bulk-heterojunction (BHJ) configuration to maximize interfacial contact and surface area (1). Specifically, BHJ solar cells based on conjugated polymer donor and fullerene acceptor blends have attracted significant research interest in the past 15 years (2–7). From the perspective of donor polymers, the rather brief history of BHJ solar cells can be roughly divided into three phases. Phase one centered on poly(phenylene vinylene)s, whose structures and related BHJ morphology were optimized to achieve an efficiency as high as 3.3% in the case of poly[2-methoxy-5-(3′,7′-dimethyloctyloxy)-1,4-phenylene vinylene] (MDMO-PPV) (8, 9). As a result of its relatively low highest-occupied molecular orbital (HOMO) energy level of −5.4 eV, BHJ devices made from MDMO-PPV offered open circuit voltages (V_{oc}) as high as 0.82 V; however, the relatively large band gap of MDMO-PPV limited the short circuit current density (J_{sc}) to 5–6 mA/cm^2. As a result, a smaller band gap polymer, regioregular poly(3-hexylthiophene) (rr-P3HT), took center stage in phase two. P3HT-based BHJ devices provided a much higher current density (> 10 mA/cm^2), which has been attributed to its relatively low band gap (1.9 eV) as well as to its increased cyrstallinity, which yields a higher hole mobility (10–12). In addition to P3HT's favorable intrinsic characteristics, important advances in materials processing at this time, such as the control of the morphology of the BHJ blend via thermal (12) or solvent annealing (13), lead to an impressive total energy conversion efficiency of 5% (6, 14). Unfortunately, the high HOMO (− 5.1 eV) energy level of P3HT has restricted the V_{oc} to 0.6 V, which consequently limits the overall efficiency. Presently, in phase three, the BHJ photovoltaic (PV) community has adopted two separate approaches to improve the efficiency of low cost BHJ PV cells. The first approach places emphasis on the V_{oc} by designing polymers with a low HOMO energy level. This approach has resulted in V_{oc} greater than 1 V in a few cases (15–17), though the overall efficiency has been less than 4% because of the mediocre J_{sc}. The second approach, which is disproportionally favored, is to develop lower band gap polymers to harvest more influx photons and enhance the J_{sc} (4, 5). By this method, J_{sc} as high as 17.5 mA/cm^2 has been achieved by poly[(4,4-didodecyldithieno[3,2-*b*:2′,3′-*d*]silole)-2,6-diyl-alt-(2,1,3-benzothiadiazole)-4,7-diyl] (**P2**) (18), demonstrating the effectiveness of low-band-gap polymers in generating more current; however, a low V_{oc} (0.57 V) was observed because of the relatively high HOMO energy level of **P2** (18). Only a few fine-tuned polymers developed recently achieved a combination of a low HOMO energy level and a small band gap, hence over 6% power conversion efficiencies were obtained (19–21).

* To whom all correspondence should be addressed. E-mail: wyou@email.unc.edu.

Received for review January 13, 2010 and accepted April 9, 2010

† Department of Chemistry, University of North Carolina at Chapel Hill.

‡ Curriculum in Applied Sciences and Engineering, University of North Carolina at Chapel Hill.

DOI: 10.1021/am1000344

2010 American Chemical Society

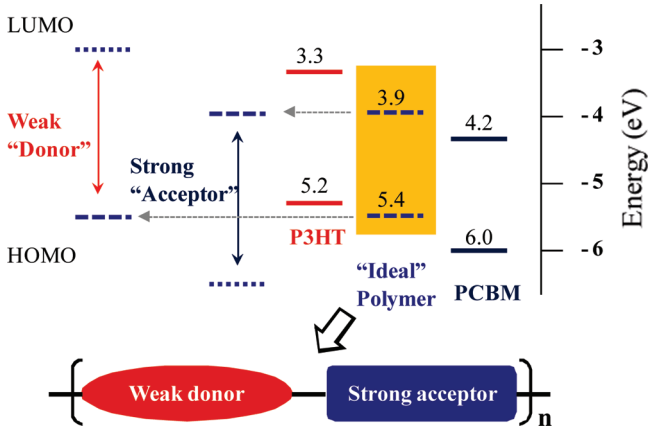

FIGURE 1. Weak donor–strong acceptor concept and energy levels.

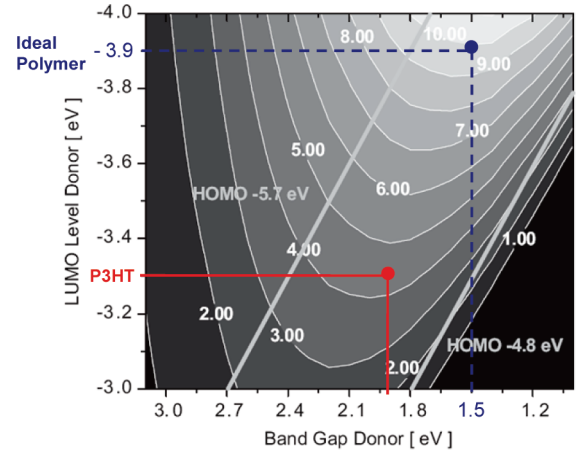

FIGURE 2. Calculated energy-conversion efficiency of P3HT and "ideal" polymer, assuming FF and IPCE at 65%. Adapted with permission from ref 22. Copyright 2006 Wiley Interscience.

To further improve the performance ($\eta = V_{oc} \times J_{sc} \times FF/P_{in}$) of polymer-based BHJ PV cells, one has to carefully address the following three issues:

(a) Open circuit voltage (V_{oc}). V_{oc} is correlated with the energy difference between the HOMO of the donor polymer and the LUMO of the acceptor (22). Therefore, the HOMO and LUMO energy levels of the donor and acceptor components need to have an optimal offset to maximize the attainable V_{oc}. Furthermore, it is estimated that a minimum energy difference of 0.3 eV between the LUMO energy levels of the donor and the acceptor is required to facilitate exciton splitting and charge dissociation. Frequently, fullerene and its derivatives (such as $PC_{61}BM$) are used as the acceptor in BHJ PV cells because of their excellent electron accepting/transporting behavior. $PC_{61}BM$ has a LUMO energy level of −4.2 eV. Therefore, the ideal lowest possible LUMO level of the donor polymer would be near −3.9 eV (Figure 1) (3). Generally, the lower the HOMO level of the donor, the higher the V_{oc} (22); however, a lower HOMO level would lead to an increased band gap in the donor polymer and less efficient light absorption.

(b) Short circuit current (J_{sc}). The theoretical upper limit for J_{sc} for a polymer solar cell is set by the number of excitons created during solar illumination. The absorption of the active layer should be compatible with the solar spectrum to maximize exciton generation. Low band gap polymers absorb more light, increasing the J_{sc}; however, lowering the band gap requires an increase of the HOMO level of donor polymer (because the LUMO level cannot be lower than −3.9 eV) and would reduce the V_{oc}. Thus, an optimal band gap of 1.5 eV is proposed to be a compromise between these two contradictory factors (22, 23). This positions the HOMO of the "ideal" polymer around −5.4 eV.

(c) Fill factor (*FF*). The morphology of the active layer governs the physical interaction between the donor polymer and the acceptor. It should be optimized to promote charge separation and favorable transport of photogenerated charges, thereby maximizing the attainable J_{sc} and *FF*.

Given the logic above, low band gap polymers are mandatory, as they better match the solar spectrum and produce higher J_{sc}. However, any low band gap polymer suitable for PV applications should also maintain a relatively low HOMO energy level to avoid any loss in the V_{oc}.

Alternating donor and acceptor units in copolymers has been proven to be an effective approach to lowering the band gap of copolymers via internal charge transfer (ICT) (24). To concurrently lower the HOMO energy level and the band gap, we propose to modify the donor–acceptor low band gap polymer strategy by constructing alternating copolymers incorporating a "weak donor" and a "strong acceptor" (Figure 1). The "weak donor" should help maintain a low HOMO energy level, while a "strong acceptor" should reduce the band gap via ICT. Assuming a fill factor of 0.65, an external quantum efficiency of 65%, and an optimal morphology, one can estimate the overall power conversion efficiency from the optical band gap and the LUMO/HOMO of donor polymers in a polymer:PCBM BHJ solar cell (Figure 2) (22). The ideal donor polymer in the BHJ device would theoretically be able to offer efficiency as high as 10%; double the efficiency (5%) of P3HT-based BHJ PV cells.

One method to design such a "weak donor" is to judiciously fuse different aromatics into polycyclic aromatics with extended conjugation. For example, one can decrease the electron-richness of the thiophene unit by fusing it with a less electron-rich benzene unit. A few such polycyclic aromatics have already been successfully applied as the weak donor in conjugated polymers yielding open circuit voltages (V_{oc}) over 0.7 V in related BHJ devices (25, 26). In this paper, another such weak donor, naphtho[2,1-*b*:3,4-*b*′]dithiophene (**NDT**) was copolymerized with a strong acceptor, benzothiadiazole (**BT**) to explore the proposed "weak donor–strong acceptor" concept. The **NDT** monomer contains a naphthalene core, which was incorporated to decrease the electron-richness of the flanked bithiophene unit. For comparison, two other polymers, the homopolymer (**HMPNDT**) and "weak donor–strong donor" polymer (**PNDT-T**) were also synthesized (see Figure 3). All three polymers were thoroughly characterized and their photovoltaic properties were carefully investigated. As expected, the "weak donor–strong acceptor" polymer, **PNDT-BT**, demonstrated both a low HOMO energy level of −5.35 eV

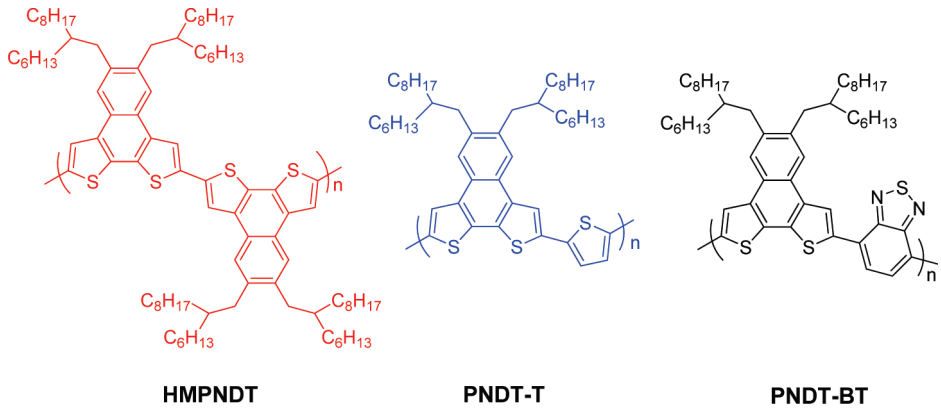

FIGURE 3. Chemical structures of HMPNDT, PNDT-T, and PNDT-BT.

Scheme 1. Polymerization of HMPNDT, PNDT-T, and PNDT-BT

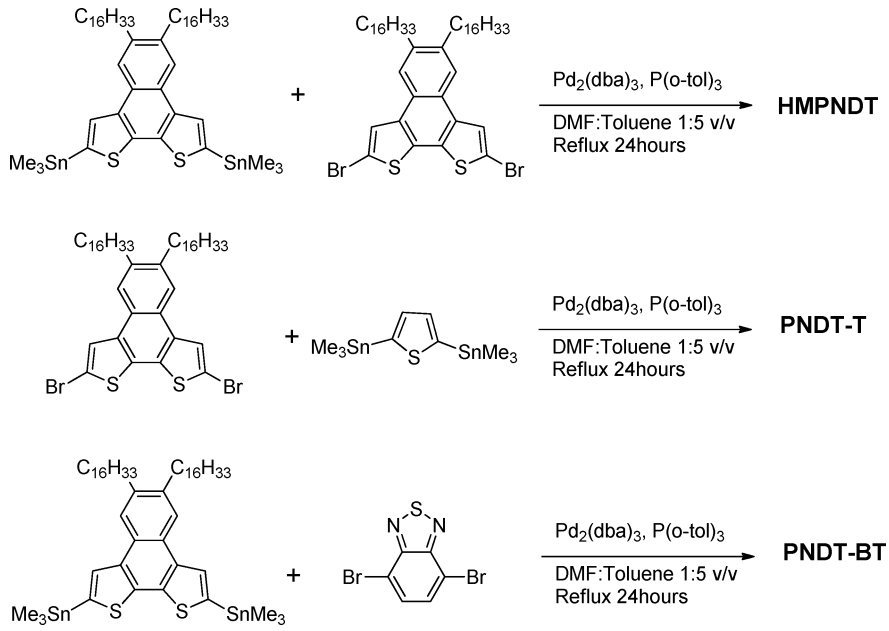

and a low band gap of 1.59 eV. A noticeably high V_{oc} of 0.83 V and a moderate J_{sc} of 2.90 mA/cm^2 were obtained from the BHJ device of **PNDT-BT** blended with PCBM, resulting in a total energy conversion efficiency of 1.27% (with a 70 nm thin film).

RESULTS AND DISCUSSION

Polymer Synthesis. Synthesis of the **NDT** monomer was described elsewhere and in the Supporting Information (27). Standard Stille coupling reactions were used to synthesize all three polymers (Scheme 1). The resulting polymers were collected by directly precipitating polymerization solutions in methanol followed by filtration. The crude polymers were extracted via a Soxhlet apparatus by methanol, followed by sequential extractions with ethyl acetate and hexane. There was no remaining polymer residue observed in the extraction thimble following hexane extraction. Hexane fractions were collected, concentrated, reprecipitated in methanol, and dried under vacuum overnight to offer the pure polymers. All purified polymers have thermal stability up to 420 °C (Table 1), and are soluble in common organic solvents such as THF and chloroform. The molecular structures of all the polymers synthesized were confirmed by NMR and element analysis (Supporting Information). Yields and molecular weights of each polymer are summarized in Table 1. Though decent yields were obtained for all three polymerizations, the molecular weight of each polymer was noticeably different. The molecular weight of **PNDT-BT** is much lower than that of **HMPNDT** or **PNDT-T**, which is assumed to be a direct result from the low reactivity of brominated benzothiadiazole in the Stille coupling polymerization (28). Therefore, further optimization of the polymerization conditions are necessary to achieve high molecular weight polymers (18).

Table 1. Polymerization Results and Thermostability of Polymers

	yield (%)	M_n[a] (kg/mol)	M_w[a] (kg/mol)	PDI[a]	T_d[b] (°C)
HMPNDT	82	16	34	2.11	426
PNDT-T	90	37	251	6.66	428
PNDT-BT	80	9	10	1.06	445

[a] Determined by GPC in tetrahydrofuran (THF) using polystyrene standards. [b] The temperature of degradation corresponding to a 5% weight loss determined by TGA at a heating rate of 10 °C/min.

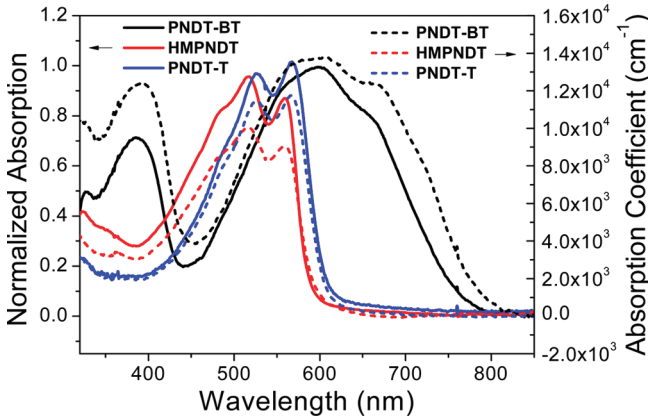

FIGURE 4. UV−vis absoption spectra of polymers in solution (solid lines) and in solid state (dash lines). The polymer films were spun coat from 5 mg/mL chloroform solution onto glass substrates.

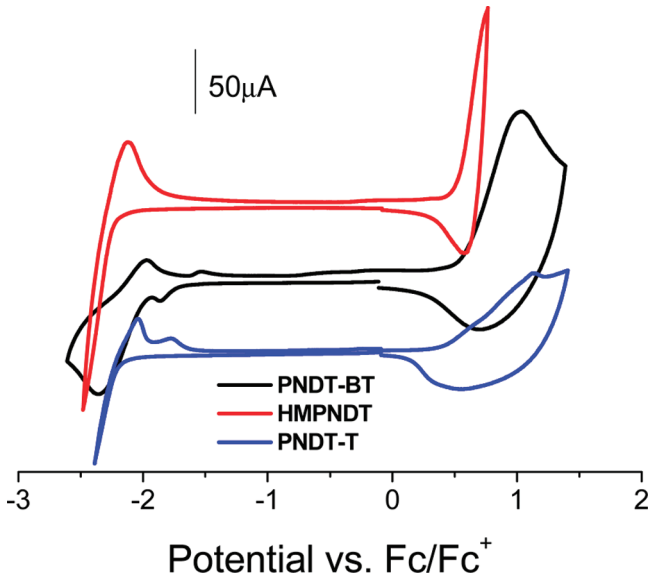

FIGURE 5. Cyclic voltammograms of the oxidation and reduction behavior of thin films of HMPNDT, PNDT-T, and PNDT-BT (HOMO and LUMO levels are calculated from the onset of the oxidation and reduction peaks, respectively).

Optical and Eletrochemical Properties. The UV−vis absorption spectra were acquired in both chloroform solution and solid state as thin films (Figure 4). The absorption coefficient of each polymer was calculated from the thin film absorption and the film thickness. HOMO and LUMO energy levels of all three polymers were estimated from cyclic voltammograms of polymer thin films drop-cast from chloroform solutions and calculated from the oxidative potential and reductive potential respectively (Figure 5). Compared with the **NDT** unit, the thiophene (**T**) unit is more electron-rich, which raises the HOMO energy level of **PNDT-T** to −5.20 eV compared with that of **HMPNDT** (−5.33 eV). Because the other common unit, **NDT**, dictates similar LUMO energy levels of **HMPNDT** and **PNDT-T**, the band gap of **PNDT-T** is slightly smaller than that of **HMPNDT** (Table 2). In similar studies, incorporating thiophene units into the polymer backbone has also shown band gap decreasing and HOMO energy level increasing (29, 30). In contrast, **PNDT-BT**, designed by the "weak donor−strong acceptor" concept, successfully demonstrates both a low HOMO energy level of −5.35 eV and a low band gap of 1.59 eV. The "weak donor", **NDT**, determines the HOMO energy level of **PNDT-BT**, explaining why a similar HOMO energy level to that of **HMPNDT** was observed. Replacing the electron-rich thiophene unit (**T**) with the highly electron-deficient benzothiadiazole unit (**BT**) effectively lowers the band gap of **PNDT-BT** to 1.59 eV via ICT. In addition, this strong internal charge transfer interaction between **NDT** and **BT** would encourage the polymer backbone to adopt a more planar structure, thereby enhancing the inter-chain stacking of polymers (31). As seen from Figure 4, a red shift in solid state absorption of **PNDT-BT** is observed compared with that of the solution absorption. Furthermore, the intensity of the "shoulder" around 680 nm noticeably increased, indicative of a pronounced interchain interaction in the solid state.

Photovoltaic Properties. The photovoltaic performance of all three polymers were probed by fabricating BHJ solar cells with the configuration of ITO/PEDOT:PSS/polymer:PCBM/Ca/Al. Device optimizations were conducted by varying solvents, ratios of polymer vs. PCBM, and film thicknesses (see the Supporting Information). Representative results for each polymer are summarized in Table 3.

Clearly, a lower HOMO energy level provides a higher open circuit voltage (V_{oc}). For example, the measured difference (0.15 eV) of the HOMO energy levels between **PNDT-T** and **PNDT-BT** almost completely translated into the observed difference in V_{oc} (~0.1 V), re-emphasizing the importance of a low HOMO energy level towards a higher V_{oc}. Because **HMPNDT** has a similar HOMO level (−5.33 eV) to that of **PNDT-BT** (−5.35 eV), a similar V_{oc} (0.83 V) was observed in **HMPNDT**-based BHJ devices (see Figure 6).

The short circuit current (J_{sc}) is a more complicated issue. Lower band gap, in theory, should harvest more light and generate higher current. However, there are other important influencing factors in BHJ devices such as the molecular weight of the polymers (18), charge carrier mobility (32, 33), and device morphology (34). Compared to **HMPNDT**, the J_{sc} of **PNDT-T** is noticeably higher, partly because of its smaller band gap. More importantly, the molecular weight of **PNDT-T** is significantly higher than that of **HMPNDT** (Table 2), which should contribute positively to the observed higher current (18). With a small band gap of 1.59 eV, **PNDT-BT** should have offered the highest J_{sc} among the three polymers. However, the maximum J_{sc} obtained through device optimization was 3 mA/cm^2. Two possible reasons account for such a low current: (a) there is only 20 wt % of **PNDT-BT** in the optimized device with a very thin active layer of 70 nm. Such a low loading of light absorbing polymers cannot absorb the incident light effectively (Figure 7); (b) the molecular weight of **PNDT-BT** is the lowest (M_n: 9 kg/mol). Usually low-molecular-weight polymers are not able to achieve the maximum current as promised by their optical band gap (35−38). This observation reiterates the necessity of a high-molecular-weight polymer in achieving a high J_{sc}.

These optimized devices were subsequently characterized for the incident photon to current efficiency (IPCE). In addition, UV−vis measurements of the active layers were

Table 2. Optical and Electrochemical Data of All Polymers

	UV−vis absorption						PL	cyclic voltammetry	
	$CHCl_3$ solution			film			$CHCl_3$ solution	E^{ox}_{onest}(V)	E^{red}_{onest}(V)
polymer	λ_{max} (nm)	λ_{onset} (nm)	$E_g{}^a$ (eV)	λ_{max} (nm)	λ_{onset} (nm)	$E_g{}^a$ (eV)	λ_{max} (nm)	HOMO (eV)	LUMO (eV)
HMPNDT	516, 561	587	2.11	515, 559	592	2.12	543, 573	0.53/−5.33	−2.23/−2.57
PNDT-T	526, 567	606	2.05	524, 567	607	2.05	544	0.40/−5.20	−2.17/−2.63
PNDT-BT	597	765	1.62	602	778	1.59	636	0.55/−5.35	−1.70/−3.1

[a] Calculated from the intersection of the tangent on the low energetic edge of the absorption spectrum with the baseline.

Table 3. PV Performances of Polymers in Optimized Conditions

polymer	polymer: PCBM (wt)	processing solvent	thickness (nm)	V_{oc} (V)	J_{sc} (mA/cm^2)	*FF*	η (%)	IPCE (%)	R_s (Ω)
HMPNDT	1:1	$CHCl_3$	65	0.83	1.42	0.47	0.56	13.3	78.5
PNDT-T	1:2	CB	55	0.73	3.25	0.50	1.18	20.1	133
PNDT-BT	1:4	CB	70	0.83	2.90	0.53	1.27	16.8	68.5

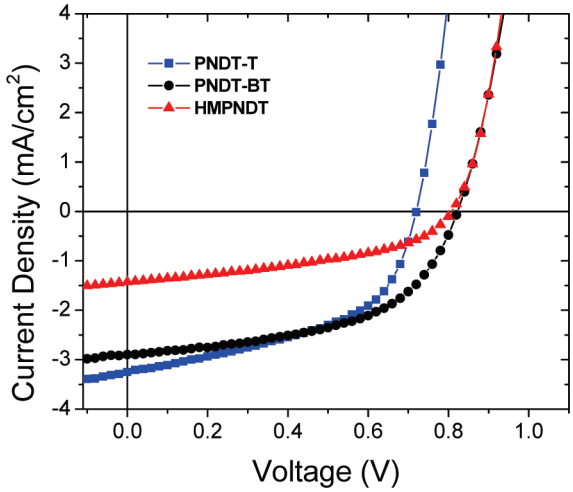

FIGURE 6. Characteristic $J-V$ curves of the optimized devices of all polymers based BHJ solar cells under 1 Sun condition (100 mW/cm^2).

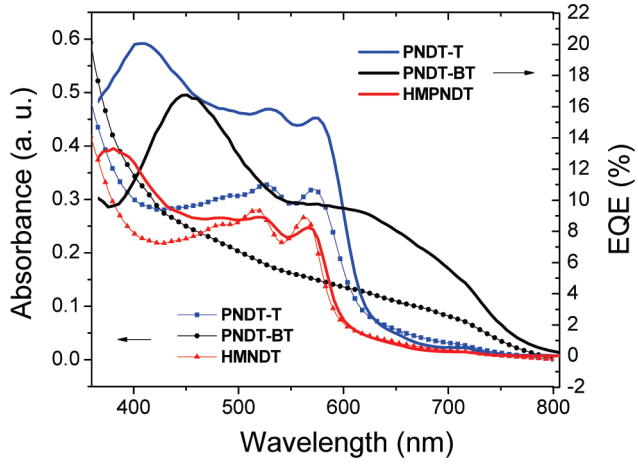

FIGURE 7. IPCE and absorption of HMNDT, PNDT-T, and PNDT-BT (absorption is normalized by film thickness).

performed on glass substrates coated with blends of polymer/PCBM prepared under the same conditions as the optimized devices. Both the UV−vis and IPCE curves are displayed together in Figure 7 to show their correlation. The high loading of PCBM in the **PNDT-BT**:PCBM blend essentially dominates the IPCE and the film absorption, resulting a peak external quantum efficiency (EQE) of 16% around 440 nm where PCBM absorbs most of the solar influx. The EQE is only about 10% in the longer wavelength region where **PNDT-BT** absorbs. On the other hand, the UV−vis spectra of **HMPNDT** and **PNDT-T** based devices with much lower loading of PCBM clearly show characteristic absorption from polymers. Still, the maximum EQE of the **PNDT-T** based device is about 20% at 400 nm, falling into the absorption region of PCBM, though higher EQE (~16%) was observed in the absorption region of **PNDT-T** (450−600 nm). With an equal weight percentage, the **HMPNDT**/PCBM (1:1) device achieves an EQE of roughly 10% across its absorption region (350−600 nm).

The investigation of the hole mobility of all these polymers provides further insights in understanding their PV performance. The space charge limited current (SCLC) method was employed to probe the vertical hole transport through the device by fabricating hole-only devices. The hole mobility of all three polymers (either in the blend or in pure polymer) are generally very low, on the order of 1×10^{-6} cm^2/(V · s) (Table 4). Such low hole mobilities require a thin film (< 100 nm) to be used, in order to effectively transport generated charges (25). Additionally, the low hole mobility of **PNDT-BT** may also explain why a much higher PCBM loading (80 wt %) is required to improve the morphology and (possibly) increase the hole mobility in the **PNDT-BT**/PCBM blend, similar to what was observed for MDMO-PPV (8, 9). The results on the mobility study indicate that the hole mobility needs to be much improved to match the electron mobility of PCBM (~1×10^{-3} cm^2/(V · s)). A balanced charge transport (electrons and holes) would minimize the build-up of space charges, thereby enhancing the observed J_{sc} (32).

CONCLUSIONS

We have demonstrated that the proposed "weak donor−strong acceptor" strategy is an effective method to achieve low band gap polymers coupled with low HOMO energy levels. This strategy takes us one step closer towards the development of ideal donor polymers to be used in conjunction with PCBM to improve the efficiency of BHJ PV cells. The "weak donor" can be prepared by judiciously fusing different aromatic units, as shown in the case of naph-

Table 4. Mobility of Polymers under SCLC Condition

polymer only	thickness (nm)	mobility ($cm^2/(V \cdot s)$)[a]	polymer: PCBM	thickness (nm)	mobility ($cm^2/(V \cdot s)$)[b]
HMPNDT	45	1.81×10^{-6}	1:1	75	6.87×10^{-6}
PNDT-T	60	4.35×10^{-6}	1:2	70	5.55×10^{-6}
PNDT-BT	50	2.60×10^{-6}	1:4	70	6.23×10^{-6}

[a] Measured with polymer-only devices with Al as the top electrode. [b] Measured with BHJ devices with Pd as the top electrode.

tho[2,1-*b*:3,4-*b*′]dithiophene (**NDT**), while the "strong acceptor" is usually supplied by electron-withdrawing conjugated aromatics, such as benzothiadiazole (**BT**). For example, **PNDT-BT**, designed under the "weak donor−strong acceptor" strategy, was able to achieve a low HOMO energy level of −5.35 eV and a narrow band gap of 1.59 eV, leading to an impressive open circuit voltage of 0.83 V. However, the short circuit current (∼ 3 mA/cm^2) was significantly lower than the maximum achievable current from such a low band gap, which limited the observed efficiency to 1.27%. Therefore, new strategies need to be actively pursued in order to (a) increase molecular weight (39) and (b) improve the hole mobility (26), in addition to maintaining a low HOMO energy level and a narrow band gap of these donor polymers.

EXPERIMENTAL SECTION

Reagents and Instrumentation. All reagents and chemicals were purchased from commercial sources (Aldrich, Acros, Strem, Fluka) and used without further purification unless stated otherwise. Reagent grade solvents were dried when necessary and purified by distillation. Gel permeation chromatography (GPC) measurements were performed on a Waters 2695 Separations Module apparatus with a differential refractive index detector with tetrahydrofuran (THF) as eluent. The obtained molecular weight is relative to the polystyrene standard. Thermogravimetric analysis (TGA) measurements were carried out with a PerkinElmer thermogravimetric analyzer (Pyris 1 TGA) at a heating rate of 10 °C min^{-1} under a nitrogen atmosphere. The temperature of degradation (T_d) is correlated to a 5% weight loss. Differential scanning calorimetry (DSC) measurements were carried out with a module Q 200 from TA Instruments under a nitrogen atmosphere. ^{1}H nuclear magnetic resonance (NMR) measurements were recorded either with a Bruker Avance 300 MHz AMX or Bruker 400 MHz DRX spectrometer. ^{13}C nuclear magnetic resonance (NMR) measurements were carried out with a Bruker 400 MHz DRX spectrometer. Chemical shifts were expressed in parts per million (ppm), and splitting patterns are designated as s (singlet), d (doublet), and m (multiplet). Coupling constants J are reported in Hertz (Hz). Element analysis was performed in Atlantic Microlab, Inc. with ±0.3% error limits for both accuracy and precision.

Electrochemistry. Cyclic voltammetry measurements were carried out using a Bioanalytical Systems (BAS) Epsilon potentiostat equipped with a standard three-electrode configuration. Typically, a three electrodes cell equipped with a glass carbon working electrode, a $Ag/AgNO_3$ (0.01M in anhydrous acetonitrile) reference electrode, and a Pt wire counter electrode was employed. The measurements were done in anhydrous acetonitrile with tetrabutyl ammonium hexafluorophosphate (0.1 M) as the supporting electrolyte under an argon atmosphere at a scan rate of 100 mV/s. Polymer films were drop cast onto the glassy carbon working electrode from a 2.5 mg/mL chloroform solution and dried under house nitrogen stream prior to measurements. The electrochemical onsets were determined at the position where the current starts to differ from the baseline. The potential of $Ag/AgNO_3$ reference electrode was internally calibrated by using the ferrocene/ferrocenium redox couple (Fc/Fc^+), which has a known reduction potential of −4.8e V (40, 41) The highest occupied molecular orbital (HOMO) and lowest unoccupied molecular orbital (LUMO) energy levels of copolymers were calculated from the onset oxidation potentials (E^{ox}_{onset}) and onset reductive potentials (E^{red}_{onset}), respectively, according to eqs 1 and 2. The electrochemically determined band gaps were deduced from the difference between onset potentials from oxidation and reduction of copolymers as depicted in eq 3.

$$\text{HOMO} = -(E^{ox}_{onset} + 4.8)\ (\text{eV}) \quad (1)$$

$$\text{LUMO} = -(E^{ox}_{onset} + 4.8)\ (\text{eV}) \quad (2)$$

$$E^{EC}_{gap} = E^{ox}_{onset} - E^{red}_{onset} \quad (3)$$

Spectroscopy. UV−visible absorption spectra were obtained by a Shimadzu UV-2401PC spectrophotometer. Fluorescence spectra were recorded on a Shimadzu RF-5301PC spectrofluorophotometer. For the measurements of thin films, polymers were spun coated onto precleaned glass slides from 10 mg/mL polymer solutions in chloroform. The thicknesses of films were recorded by a profilometer (Alpha-Step 200, Tencor Instruments).

Polymer Solar Cell Fabrication and Testing. Glass substrates coated with patterned indium-doped tin oxide (ITO) were purchased from Thin Film Devices, Inc. The 150 nm sputtered ITO pattern had a resistivity of 15Ω/□. Prior to use, the substrates were ultrasonicated in acetone followed by deionized water and then 2-propanol for 20 min each. The substrates were dried under a stream of nitrogen and subjected to the treatment of UV-Ozone over 30 minutes. A 0.45 μm filtered dispersion of PEDOT:PSS in water (Baytron PH500) was then spun cast onto clean ITO substrates at 4000 rpm for 60 s and then baked at 140 °C for 15 min to give a thin film with a thickness of 40 nm. A blend of polymer and PCBM with varied concentration and feed ratio were dissolved in organic solvent with heating at 90 °C for 6 h. All the solutions were filtered through a 0.45 μm poly(tetrafluoroethylene) (PTFE) filter, spun cast at different rpm for 60 seconds onto PEDOT:PSS layer. The substrates were then dried under a vacuum at room temperature for 12 h. The thicknesses of films were recorded by a profilometer (Alpha-Step 200, Tencor Instruments). The devices were finished for measurement after thermal deposition of a 25 nm film of calcium and a 80 nm aluminum film as the cathode at a pressure of $\sim 1 \times 10^{-6}$ mbar. There are 8 devices per substrate, with an active area of 12 mm^2 per device. Device characterization was carried out under AM 1.5G irradiation with the intensity of 100 mW/cm^2 (Oriel 91160, 300 W) calibrated by a NREL certified standard silicon cell. Current versus potential ($I-V$) curves were recorded with a Keithley 2400 digital source meter. EQE were detected under monochromatic illumination (Oriel Cornerstone 260 1/4 m monochromator equipped with Oriel 70613NS QTH lamp) and the calibration of the incident light was performed with a monocrystalline silicon diode. All fabrication steps after adding the PEDOT:PSS layer onto ITO substrate,

and characterizations were performed in gloveboxes under nitrogen atmosphere. For mobility measurements, the hole-only devices in a configuration of ITO/PEDOT:PSS (40 nm)/copolymer-PCBM/Pd (50 nm) were fabricated. The experimental dark current densities J of polymer:PCBM blends were measured when applied with voltage from 0 to 6 V. The applied voltage V was corrected from the built-in voltage V_{bi}, which was taken as a compensation voltage $V_{bi} = V_{oc} + 0.05$ V and the voltage drop V_{rs} across the indium tin oxide/poly(3,4-ethylenedioxythiophene):poly(styrene sulfonic acid) (ITO/PEDOT:PSS) series resistance and contact resistance, which is found to be around 35 Ω from a reference device without the polymer layer. From the plots of $J^{0.5}$ vs V (see the Supporting Information), hole mobilities of copolymers can be deduced from

$$J = \frac{9}{8}\varepsilon_r\varepsilon_0\mu_h\frac{V^2}{L^3}$$

where ε_0 is the permittivity of free space, ε_r is the dielectric constant of the polymer which is assumed to be around 3 for the conjugated polymers, μ_h is the hole mobility, V is the voltage drop across the device, and L is the film thickness of active layer.

Acknowledgment. This work was supported by the University of North Carolina at Chapel Hill, a DuPont Young Professor Award, ONR (Grant N000140911016), and NSF CAREER Award (DMR-0954280).

Supporting Information Available: Synthesis of monomers and polymers; NMR data of monomers and polymers; fluorescence spectra of all polymers; TGA and DSC curves; $J^{0.5}$ vs V plots of mobility measurement of all polymers; PV data of selected devices. This material is available free of charge via the Internet at http://pubs.acs.org.

REFERENCES AND NOTES

(1) Yu, G.; Gao, J.; Hummelen, J. C.; Wudl, F.; Heeger, A. J. *Science* **1995**, *270*, 1789–1791.
(2) Gunes, S.; Neugebauer, H.; Sariciftci, N. S. *Chem. Rev.* **2007**, *107*, 1324–1338.
(3) Thompson, B. C.; Fréchet, J. M. J. *Angew. Chem., Int. Ed.* **2008**, *47*, 58–77.
(4) Kroon, R.; Lenes, M.; Hummelen, J. C.; Blom, P. W. M.; de Boer, B. *Polym. Rev.* **2008**, *48*, 531–582.
(5) Bundgaard, E.; Krebs, F. C. *Sol. Energy Mater. Sol. Cells* **2007**, *91*, 954–985.
(6) Dennler, G.; Scharber, M. C.; Brabec, C. J. *Adv. Mater.* **2009**, *21*, 1323–1338.
(7) Chen, J.; Cao, Y. *Acc. Chem. Res.* **2009**, *42*, 1709–1718.
(8) Shaheen, S. E.; Brabec, C. J.; Sariciftci, N. S.; Padinger, F.; Fromherz, T.; Hummelen, J. C. *Appl. Phys. Lett.* **2001**, *78*, 841–843.
(9) Brabec, C. J.; Shaheen, S. E.; Winder, C.; Sariciftci, N. S.; Denk, P. *Appl. Phys. Lett.* **2002**, *80*, 1288–1290.
(10) Reyes-Reyes, M.; Kim, K.; Carroll, D. L. *Appl. Phys. Lett.* **2005**, *87*, 3.
(11) Kim, J. Y.; Kim, S. H.; Lee, H. H.; Lee, K.; Ma, W. L.; Gong, X.; Heeger, A. J. *Adv. Mater.* **2006**, *18*, 572+.
(12) Ma, W. L.; Yang, C. Y.; Gong, X.; Lee, K.; Heeger, A. J. *Adv. Funct. Mater.* **2005**, *15*, 1617–1622.
(13) Li, G.; Shrotriya, V.; Huang, J. S.; Yao, Y.; Moriarty, T.; Emery, K.; Yang, Y. *Nat. Mater.* **2005**, *4*, 864–868.
(14) Kim, Y.; Cook, S.; Tuladhar, S. M.; Choulis, S. A.; Nelson, J.; Durrant, J. R.; Bradley, D. D. C.; Giles, M.; McCulloch, I.; Ha, C.-S.; Ree, M. *Nat. Mater.* **2006**, *5*, 197–203.
(15) Gadisa, A.; Mammo, W.; Andersson, L. M.; Admassie, S.; Zhang, F.; Andersson, M. R.; Inganäs, O. *Adv. Funct. Mater.* **2007**, *17*, 3836–3842.
(16) Zhang, F.; Jespersen, K. G.; Björström, C.; Svensson, M.; Andersson, M. R.; Sundström, V.; Magnusson, K.; Moons, E.; Yartsev, A.; Inganäs, O. *Adv. Funct. Mater.* **2006**, *16*, 667–674.
(17) Andersson, L. M.; Zhang, F.; Inganäs, O. *Appl. Phys. Lett.* **2007**, *91*, 071108.
(18) Coffin, R. C.; Peet, J.; Rogers, J.; Bazan, G. C. *Nat. Chem.* **2009**, *1*, 657–661.
(19) Park, S. H.; Roy, A.; Beaupre, S.; Cho, S.; Coates, N.; Moon, J. S.; Moses, D.; Leclerc, M.; Lee, K.; Heeger, A. J. *Nat. Photonics* **2009**, *3*, 297–302.
(20) Liang, Y. Y.; Feng, D. Q.; Wu, Y.; Tsai, S. T.; Li, G.; Ray, C.; Yu, L. P. *J. Am. Chem. Soc.* **2009**, *131*, 7792–7799.
(21) Chen, H.-Y.; Hou, J.; Zhang, S.; Liang, Y.; Yang, G.; Yang, Y.; Yu, L.; Wu, Y.; Li, G. *Nat. Photonics* **2009**, *3*, 649–653.
(22) Scharber, M. C.; Mühlbacher, D.; Koppe, M.; Denk, P.; Waldauf, C.; Heeger, A. J.; Brabec, C. J. *Adv. Mater.* **2006**, *18*, 789–794.
(23) Soci, C.; Hwang, I. W.; Moses, D.; Zhu, Z.; Waller, D.; Gaudiana, R.; Brabec, C. J.; Heeger, A. J. *Adv. Funct. Mater.* **2007**, *17*, 632–636.
(24) Roncali, J. *Chem. Rev.* **1997**, *97*, 173–205.
(25) Xiao, S.; Stuart, A. C.; Liu, S.; You, W. *ACS Appl. Mater. Interfaces* **2009**, *1*, 1613–1621.
(26) Xiao, S.; Stuart, A. C.; Liu, S.; Zhou, H.; You, W. *Adv. Funct. Mater.* **2010**, *20*, 635–643.
(27) Xiao, S. Q.; Zhou, H. X.; You, W. *Macromolecules* **2008**, *41*, 5688–5696.
(28) Zhang, M.; Tsao, H. N.; Pisula, W.; Yang, C.; Mishra, A. K.; Müllen, K. *J. Am. Chem. Soc.* **2007**, *129*, 3472–3473.
(29) Price, S. C.; Stuart, A. C.; You, W. *Macromolecules* **2009**, *43*, 797–804.
(30) Hou, J.; Park, M.-H.; Zhang, S.; Yao, Y.; Chen, L.-M.; Li, J.-H.; Yang, Y. *Macromolecules* **2008**, *41*, 6012–6018.
(31) Kim, Y.; Cook, S.; Tuladhar, S. M.; Choulis, S. A.; Nelson, J.; Durrant, J. R.; Bradley, D. D. C.; Giles, M.; McCulloch, I.; Ha, C. S.; Ree, M. *Nat. Mater.* **2006**, *5*, 197–203.
(32) Mandoc, M. M.; Koster, L. J. A.; Blom, P. W. M. *Appl. Phys. Lett.* **2007**, *90*, 133504.
(33) Kirchartz, T.; Pieters, B. E.; Taretto, K.; Rau, U. *J. Appl. Phys.* **2008**, *104*, 094513.
(34) Moulé, A. J.; Meerholz, K. *Adv. Funct. Mater.* **2009**, *19*, 3028–3036.
(35) Schilinsky, P.; Asawapirom, U.; Scherf, U.; Biele, M.; Brabec, C. J. *Chem. Mater.* **2005**, *17*, 2175–2180.
(36) Ma, W.; Kim, J. Y.; Lee, K.; Heeger, A. J. *Macromol. Rapid Commun.* **2007**, *28*, 1776–1780.
(37) Ballantyne, A. M.; Chen, L.; Dane, J.; Hammant, T.; Braun, F. M.; Heeney, M.; Duffy, W.; McCulloch, I.; Bradley, D. D. C.; Nelson, J. *Adv. Funct. Mater.* **2008**, *18*, 2373–2380.
(38) Morana, M.; Wegscheider, M.; Bonanni, A.; Kopidakis, N.; Shaheen, S.; Scharber, M.; Zhu, Z.; Waller, D.; Gaudiana, R.; Brabec, C. *Adv. Funct. Mater.* **2008**, *18*, 1757–1766.
(39) Zhou, H.; Yang, L.; Xiao, S.; Liu, S.; You, W. *Macromolecules* **2010**, *43*, 811–820.
(40) Pommerehne, J.; Vestweber, H.; Guss, W.; Mahrt, R. F.; Bassler, H.; Porsch, M.; Daub, J. *Adv. Mater.* **1995**, *7*, 551–554.
(41) Zhan, X. W.; Liu, Y. Q.; Wu, X.; Wang, S. A.; Zhu, D. B. *Macromolecules* **2002**, *35*, 2529–2537.

AM1000344